

Article

Analysis of the Mechanical Performance of Sleeve Considering the Different Distributions of Grouting Defects

Jun Zhao ¹, Lulu Yin ², Jing Chen ², Yizhou Yang ², Yinhong Zhu ^{2,*} and Bai Yang ^{1,*} ¹ School of Architecture and Transportation Engineering,

Guilin University of Electronic Technology, Guilin 541004, China; zhaojun@guet.edu.cn

² College of Civil Engineering and Architecture, Guilin University of Technology, Guilin 541004, China;

luluyin1996@gmail.com (L.Y.); chenjing9711@gmail.com (J.C.); yump6868@gmail.com (Y.Y.)

* Correspondence: zyh6130@163.com (Y.Z.); ayangbai@163.com (B.Y.)

Abstract: To study the influence of grouting defects on the mechanical properties of grouting sleeves, 49 groups of specimens with different specifications were made considering the length and location of defects, monotonic axial tension tests were carried out to study the influence of grouting defects on its failure process, failure mode, load-displacement curve, bearing capacity and other mechanical properties, and the influence law of different distribution defects on the grouting sleeve was analyzed. This research shows that there are two forms of sleeve failure: steel bar fracture failure and steel bar pullout failure. The bearing capacity of specimens with a defect length of 2D and 3D varies with the defect type. The ultimate displacement of specimens with a defect length of 2D varies with the defect type. The ultimate displacement of specimens with a defect length of 3D increases with the increase in bearing capacity. By moving defects, it is found that if there is a vertical overlap of defects in the upper or middle part of the specimen, the bearing capacity of the specimen will be greatly affected.

Keywords: grouting sleeve; grouting defect; monotonic tensile test; ultimate bearing capacity



Citation: Zhao, J.; Yin, L.; Chen, J.; Yang, Y.; Zhu, Y.; Yang, B. Analysis of the Mechanical Performance of Sleeve Considering the Different Distributions of Grouting Defects. *Buildings* **2023**, *13*, 2873. <https://doi.org/10.3390/buildings13112873>

Academic Editor: Chuang Feng

Received: 29 September 2023

Revised: 7 November 2023

Accepted: 11 November 2023

Published: 16 November 2023



Copyright: © 2023 by the authors. Licensee MDPI, Basel, Switzerland. This article is an open access article distributed under the terms and conditions of the Creative Commons Attribution (CC BY) license (<https://creativecommons.org/licenses/by/4.0/>).

1. Introduction

Sleeve grouting connection technology is the core technology of the joint connection of prefabricated structures. The quality of joint connection directly affects the quality and safety of the whole prefabricated building structure. Whether there are defects in the splicing surface between different components also directly affects the connection quality of joints. Due to slurry leakage at the bottom of the sleeve, bubbles in the grouting material are not exhausted, and, for other reasons, various forms of defects will appear in the sleeve cavity. Once there is a defect, its mechanical performance will be reduced, causing potential safety hazards to the actual project.

Many scholars have conducted a lot of experimental studies on the defects of grouting sleeves. Ling et al. studied the mechanical properties and failure modes of sleeve connections under axial loads. The results show that the embedded length of the required splicing steel bar can be reduced by 8 times the diameter of the steel bar in the presence of constraints [1–3]. Wu et al. [4] conducted monotonic and repeated tensile tests on 36 specimens to understand the influence of grouting material age and steel bar type on the mechanical properties of grouting sleeve connectors. The test results show that the age of the grouting material at the initial stage of curing has a great influence on the bearing capacity and deformation of the connector. The type of reinforcement has no obvious effect on the deformation of the connector. Steuck et al. [5] carried out uniaxial tension on large-diameter steel bar connectors. The results show that when the anchorage length of large-diameter sleeve connectors is 6 times the diameter of steel bars, the yield strength of steel bars is reached. When the anchorage length is 10 times the diameter of the steel bar, the steel bar is pulled off to reach the ultimate strength of the steel bar. Sayadi et al. [6], in order to study the influence of the interlocking mechanism in the elastic and inelastic

sections of a sleeve on the bond strength of the sleeve, made 10 concrete beams with sleeve length, number of bolts and bolt position as variables. The research shows that if we set the interlocking mechanism in the elastic stage of the sleeve, the bond strength of the grouting sleeve and the bearing capacity of the precast concrete beam will be reduced. Chen et al. [7] made six groups of semi-grouting sleeve specimens to study the influence of the water–binder ratio of grouting material and the steel bar diameter on the mechanical properties of sleeves and carried out tensile load tests. The test results show that the displacement of the yield point and failure point, the tensile strain of the sleeve surface, and the damage depth of end grouting material increase with increases in the steel bar diameter. The high water–binder ratio leads to bond failure of the specimen and increases the damage depth of the end grouting material. Liu et al. [8] conducted a series of tensile load tests on a set of grouted sleeve joints and conducted a three-dimensional finite element analysis of the tensile test. Through the study of finite element parameters, the influence of the gap between the sleeve and the steel bar and the anchorage diameter ratio on the anchorage performance was discussed. The numerical results show that an anchorage length greater than 7 times the diameter of the steel bar is sufficient to prevent slip failure between the grouting and the steel bar. Xu et al. [9] made four kinds of specimens with grouting defects, which were uniform, longitudinal, radial and oblique, to carry out single tensile tests. The test results show that no matter the type of grouting defects, when the grouting defects exceed 30%, the failure mode of the specimen changes from the tensile fracture of the steel bar to the pull-out of the steel bar. Zheng et al. [10] made 24 sleeves with vertical grouting defects for research, considering three loading methods, namely, uniaxial tension, high stress and large deformation, while considering the influence of secondary grouting. The research shows that the loading mode has a certain influence on the failure mode. In addition, the secondary grouting sleeve connection shows similar mechanical properties to the full grouting sleeve connection. Zhang et al. [11] conducted a uniaxial tensile test on 66 semi-grouting sleeves that were not full after high temperatures. The test results show that the tensile performance of the semi-grouting sleeve is directly affected by the peak temperature and construction defects. When the temperature exceeds 600 °C, the connector will become unreliable. The influence of construction defects on the mechanical properties of the specimens depends on the weakening degree of the effective bonding area between the steel bar and the grouting material. Grouting sleeves have also become the focus of many scholars [12–17]. Gao et al. [18] studied the effect of defects of different sizes on the unidirectional tension of grouting sleeve joints by setting defects at the lower part of the grouting sleeve. Research has shown that whether it is a fully grouted sleeve or a semi-grouted sleeve, the maximum length of the middle defect is approximately 0.5–0.66 times the maximum length of the end defect while ensuring that the steel bars outside the sleeve joint are pulled off. Zheng et al. [19] conducted extensive experiments to investigate the effects of various grouting defects on the performance of sleeve grouting joint specimens and prefabricated concrete beam-column specimens to explore the effectiveness and applicability of non-destructive testing methods for grouting defects. The experimental results show that, under the premise of equivalent defect equivalence, the influence of defects in the middle of the specimen is greater than that of end defects, horizontal grouting defects are greater than vertical grouting defects, and defects in the case of eccentricity of steel bars are greater than those in the case of axial reinforcement. X-rays can clearly identify the interface between the inner wall of the sleeve and the grouting material and steel reinforcement, with a minimum identification size of 1 mm and 4 mm. The impact of grouting defects on prefabricated concrete columns is mainly to reduce the bearing capacity and ductility of the specimens. Under the premise of full grouting, the prefabricated concrete beam connected by sleeve grouting can meet the requirements of bearing capacity and ductility. Yu et al. [20] carried out tensile tests on 36 joints to study the stress mechanism of steel sleeve grouting lap joints, fitted the formula of joint ultimate bond strength, and proposed the formula of sleeve critical lap length.

To sum up, at present, the research on grouting sleeves with grouting defects is not perfect, and the research on the stress performance of sleeves by defect distribution is even less so. This paper studies the effect of different distributions of grouting defects on the mechanical properties of sleeves under uniaxial tension. The influence law is obtained through the test, which supplements the grouting defect theory.

2. Experimental Design

2.1. Design and Fabrication of Specimen

Four groups of 49 grouting sleeve specimens were made. Among them, 2 sleeve specimens were full grouting and as a group. The ring (Type H), Type A, Type B and Type C defect specimens with total defect lengths of 1D, 2D and 3D were distributed downward along the steel bar from the end of the sleeve. D represents the diameter of the steel bar and the defect thickness was 2 mm. The central circle represents the steel bar in the test piece and the part around the steel bar represents the defect. As shown in Figure 1.

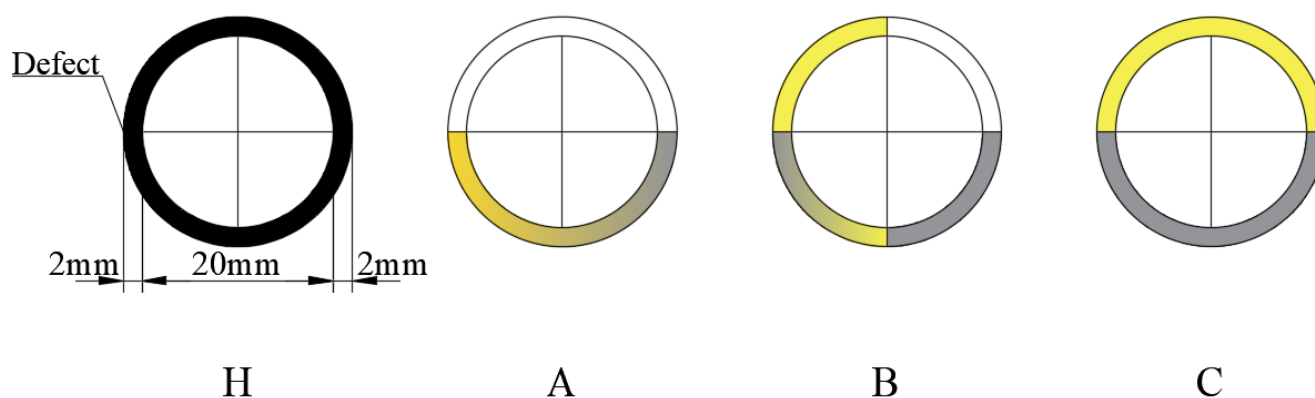


Figure 1. Top view of grouting sleeve. **Note:** The gradient color indicates that the grouting defect in this part was continuously divided along the longitudinal direction of the sleeve.

In practical engineering, the division of grouting defects is random. This experiment was conducted to study the influence of defects at different distribution positions on the mechanical properties of specimens. In order to make the defect type more comprehensive, we divided the defect into 8 equal parts (2D) or 12 equal parts (3D) while maintaining the same length of the defect and then listed the defect types by permutation and combination. In Figures 2 and 3, the black part indicates the grouting defect, the white part indicates no grouting defect and the arrow indicates the direction of the defect movement. Type A defects had a 1/2 vertical overlap and were concentrated on one side. Type B defects had a 1/4 vertical overlap and were staggered. Type C defects were only staggered without a vertical overlap. As the failure mode of specimens with a defect length of 1D and 2D in Type H was that the steel bar was broken, the test was only conducted for specimens with a defect length of 2D and 3D in other types. It is explained here that because there was no objection to the concept of full grouting and annular defect, Figures 2 and 3 show 44 specimens of Type A, Type B and Type C defects with a total length of 2D and 3D, respectively. In total, 3 specimens of annular defect (Type H) with a total length of 1D, 2D and 3D, respectively, and 2 specimens of full grouting are not shown.

The key point in the production process of specimens was the setting of grouting defects. In this test, foam tape was used to replace the defects. In order to prevent the tape from falling off during the grouting process, cotton thread was used to wind it and, finally, the specimen was grouted. After grouting, the specimen was cured for 28 days. The specific production process is shown in Figures 4 and 5.

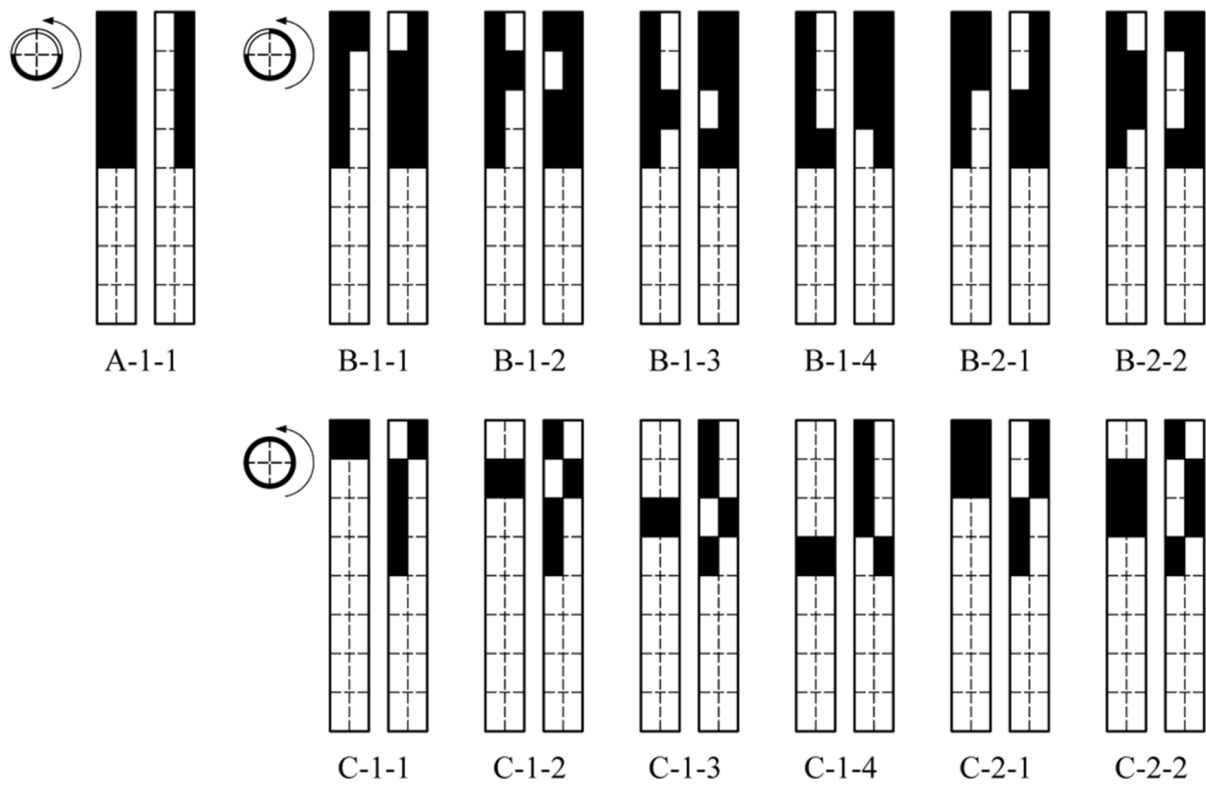


Figure 2. Diagram of specimen with total defect length of 2D.

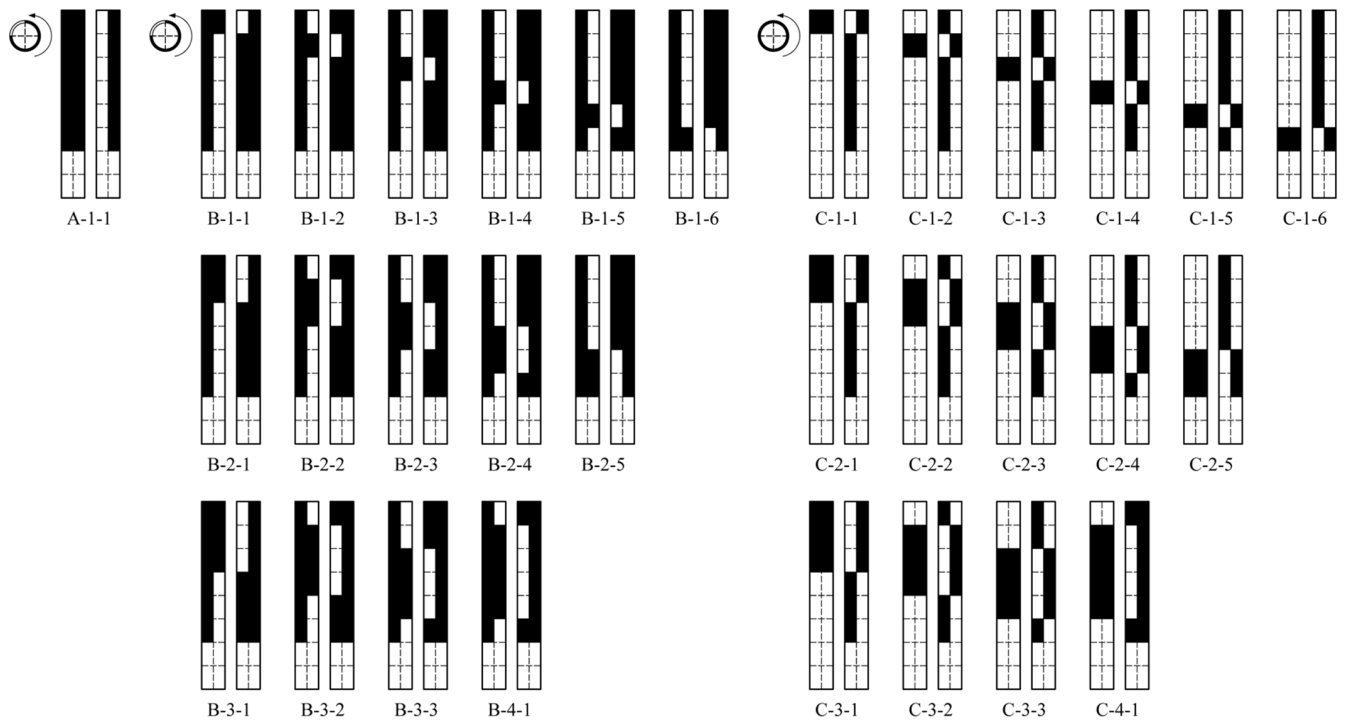


Figure 3. Diagram of specimen with total defect length of 3D.



Figure 4. Defect settings of piles.

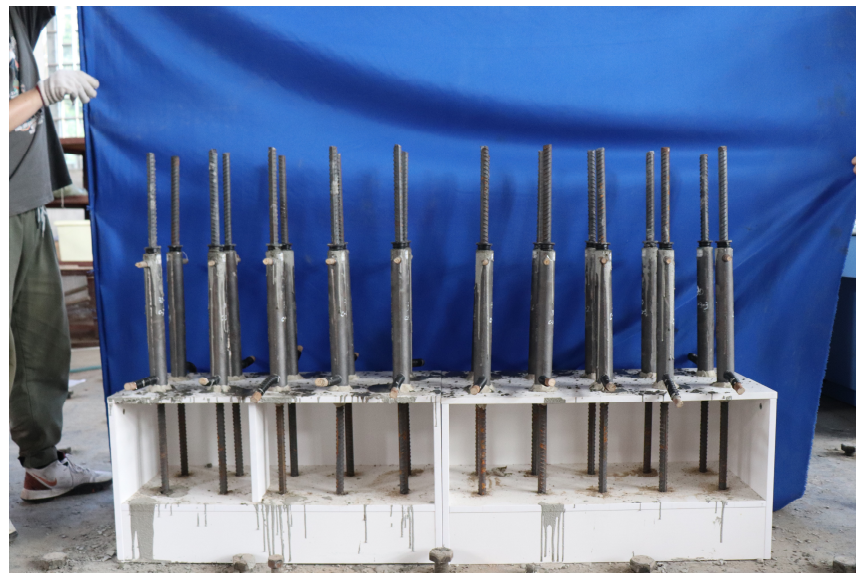


Figure 5. Profile of piles.

2.2. Material Properties and Loading Methods

Except for the self-test of the compressive strength of the grouting material and the yield strength of the steel bar, the other parameters were provided by the manufacturer. The grouting material used in the test was a finished product, which could be mixed according to the water–cement ratio provided by the manufacturer. (1) In order to verify whether the strength of the grouting material met the requirements of “sleeve grouting material for steel bar connection” JG/T408-2013, the strength of the grouting material was ≥ 85 MPa.

Therefore, three prisms with a size of 40 mm × 40 mm × 160 mm were made when making grouting sleeve connectors and their compressive strength was tested after 28 days of curing. (2) In order to verify whether the strength of the steel bar met the requirements, three steel bars used in the test were taken for drawing tests to test their yield strength and tensile strength.

The grouting material complied with the requirements of Cementitious Grout for Coupler of Rebar Splicing (JG/T408-2013) [21]. The grouting material performance parameters are shown in Table 1.

Table 1. Parameters of grouting material.

Compressive Strength/MPa	Water–Cement Ratio/(w/c)	Poisson’s Ratio	Elastic Modulus E_c /MPa
85	0.115	0.2	20,000

The steel bar was HRB400 mild steel with 20 mm diameter D and obvious flow amplitude, with a Poisson’s ratio of 0.3. The mechanical properties are shown in Table 2.

Table 2. Parameters of rebar and sleeve.

Diameter/mm	Grade	Yielding Strength f_u /MPa	Elastic Modulus E_s /MPa
20	HRB400	420	2.10×10^5
44	QT550-5	≥ 370	1.62×10^5

The ductile iron full grouting sleeve was developed by Shenzhen Modern Construction Technology Co. Its mechanical properties met the requirements of The Grouting Sleeve for Rebars Splicing (JG/T 398-2019) [22]. The material spheroidization rate was greater than 85% and its standard anchoring length was $8D$. The mechanical properties of the sleeve are shown in Table 2. The test showed that the mechanical performance of the sleeve met the requirements under the conditions of full grouting. The specific structure is shown in Figure 6.

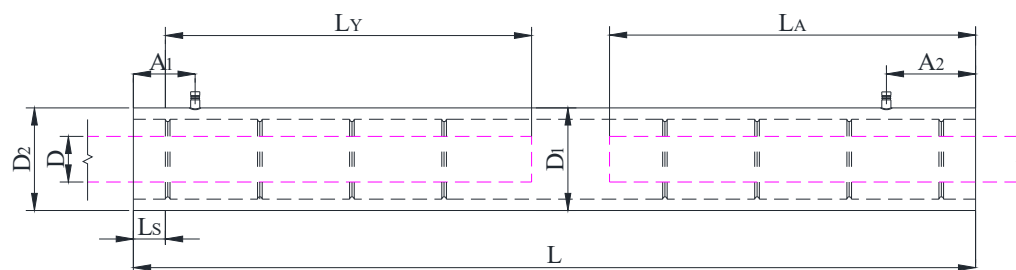


Figure 6. Structure diagram of grouting sleeve.

Figure 6 shows the structure diagram of the grouting sleeve. The left and right sides of the grouting sleeve were the grouting outlet and the grouting inlet, respectively. The length from the pre-installed end face to the anchorage calculation section was $L_S = 15$ mm. The pre-installed end anchorage length was $L_Y = 160$ mm ($8D$). The middle limit block was $B = 3$ mm. The installation end anchorage length was $L_A = 160$ mm ($8D$). The total length of the sleeve was $L = 368$ mm. The middle section’s outer diameter was $D_1 = 45$ mm. The outer diameter of both ends was $D_2 = 44$ mm. The distance between the center line of the grouting outlet and the left end face of the sleeve was $A_1 = 27$ mm and the distance between the center line of the grouting inlet and the right end face of the sleeve was $A_2 = 39$ mm. The structural parameters of the grouting sleeve are shown in Table 3.

Table 3. Structural parameters of grouting sleeve.

L/mm	L _Y /mm	L _A /mm	B/mm	A ₁ /mm	A ₂ /mm	D ₁ /mm	D ₂ /mm	D/mm
368	160	160	3	27	39	45	44	20

A uniaxial tensile test was conducted according to the requirements of Technical specification for grout sleeve splicing of rebars (JG/T355-2015) [23]. The experimental device was a hydraulic universal testing machine with a range of 1000 kN that could automatically collect force and displacement. The loading speed was set to 0.5 kN/s until the sample was damaged.

3. Test Results

3.1. Failure Modes and Phenomena

The failure mode of the grouting sleeves depended on the ultimate strength of the steel bar and the bond strength between the steel bar and the grouting material. There were two failure modes: steel bar broken and steel bar pulled out, as shown in Figure 7.



Figure 7. Failure modes: (a) steel bar pullout failure; (b) steel bar fracture failure.

The load-displacement curve of the tensile failure of the steel bar in the specimen was similar to that of uniaxial tensile failure of the steel bar. It also went through four stages: elastic stage, yield stage, strengthening stage and failure stage. From the load-displacement curve of the specimen, the load and displacement in the elastic stage had a linear relationship. Different from the load-displacement curve of the steel bar, with the increase in load, the load fluctuated only briefly in the yield stage and then entered the strengthening stage. At the strengthening stage, the load-displacement curve rose gently, and its slope gradually decreased to 0. After that, the steel bar at the end of the specimen through necking and further loading led to the fracture of the steel bar.

When the pullout failure occurred, the elastic stage and yield stage were consistent with the tensile failure of the steel bar, and there were obvious differences from the strengthening stage and the failure stage. In the strengthening stage, the ultimate bearing capacity of the specimen varied with the defect type and distribution. In the failure stage, the steel bar slip was small at the beginning and the bearing capacity decreased slightly. When the shear stress of the grouting material reached the ultimate bond strength, the steel bar was finally pulled out. The failure displacement of the specimen included two parts: one was the yield displacement of the steel bar at yield and the other was the bond slip of the steel bar.

3.2. Model Establishment and Boundary Conditions

3.2.1. Annular Defect Specimen

The four curves in Figure 8a represent the load-displacement curves of full grouting and annular defects of different lengths, respectively. Just as shown in Figure 8b, when the deficiency lengths were 1D and 2D, the failure mode of the test sample was that the steel bar was pulled apart. When the deficiency length was 3D, the limit bearing capacity of the sleeve was 185.3 kN; after that, the steel bar was pulled out.

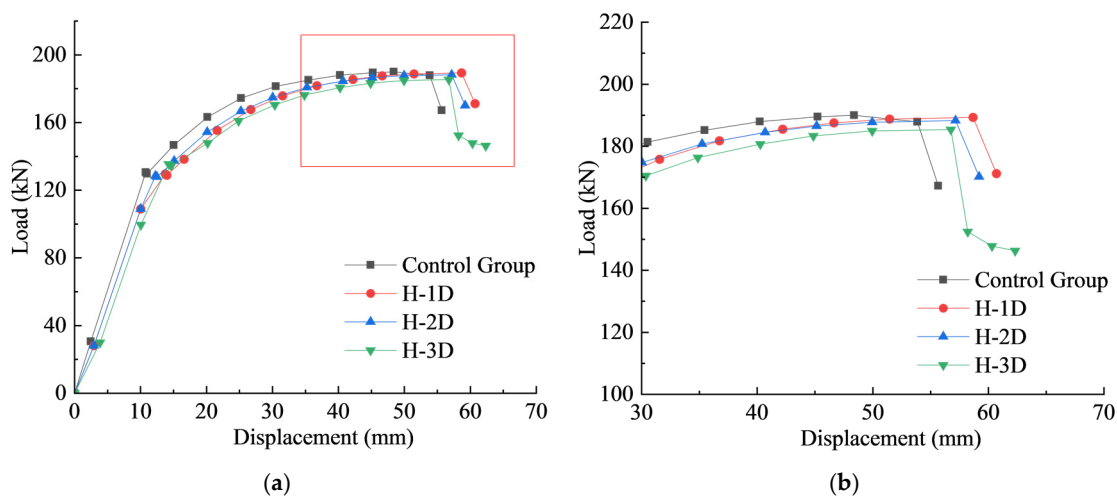


Figure 8. Load-displacement curve of annular defect specimen: (a) type H and control group specimens; (b) attachment.

In the elastic stage, the load values of specimens with defects were almost the same, and the slope of the load-displacement curve of specimens without grouting defects was slightly greater than that of others. The yield load of each specimen was about 130 kN. When the specimen went to the strengthening stage, the bearing capacity of the test sample decreased with the increase in the defect length. The limit bearing capacity of the H-1D specimen was similar to that of the H-2D specimen, and the displacement of the H-1D specimen increased by 6 mm and 4 mm, respectively, compared with that of the flawless specimen. The limit bearing capacity of the H-3D specimen was less than that of the control group. In the descending section, both H-1D and H-2D specimens were approximately a straight line. In the early stage, the H-3D specimen was a straight line, and in the late stage, the curve slope decreased gradually.

3.2.2. Specimen with Defect Length of 2D

Through the tests of various specimens with a defect length of 2D, we can observe that the failure pattern of the test sample was that the steel bar was broken. As shown in Figure 9, in the elastic stage, the curve of four types of defects almost coincided. And the yield load values of type H, type A and type B defects were basically the same, but they were slightly smaller than that of type C defects. At the yield stage, the yield load values of specimens 2D-A-1-1, 2D-B-1-1 and 2D-C-1-1 were slightly lower than that of H-2D. The bearing capacity in the strengthening stage basically showed as type A < B < C ≈ H. Under the same displacement, the bearing capacity of specimens with type H and type C defects was bigger, while the bearing capacity of specimens with type A defects was the smallest. Under the same proportion of defects, the bearing capacity of defects concentrated on one side was weaker. This is because the vertical concentrated defects reduced the mechanical biting force and chemical bonding force of the steel bar and grouting material, which reduced the ultimate bond strength of the specimen.

As shown in Figure 10, in the case of a single moving defect, the linear segments of the four curves almost coincided. In the yield stage, except the yield load value of the 2D-B-1-3 specimen being larger, the other specimens were slightly lower. In the strengthening stage, the slope of the load-displacement curve of the whole specimen changed rapidly. There was a great difference between the 2D-B-1-2 specimen and the 2D-B-1-4 specimen, but the ultimate bearing capacity was roughly the same, with an average value of 184.24 kN, and the average displacement corresponding to the ultimate load was 52.1 mm. The limit bearing capacity of the four test samples was less than the ultimate tensile strength of the control group, and the steel bars of the test samples were all pulled out.

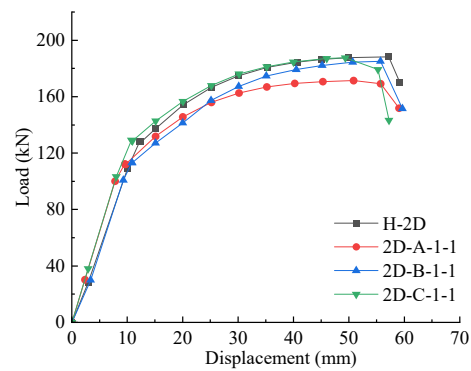


Figure 9. Comparison of load-displacement curves of various specimens (2D).

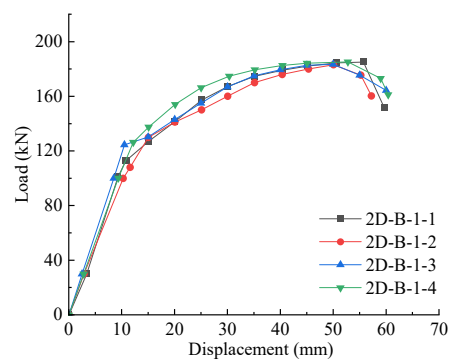


Figure 10. Load-displacement curve of type B-1 specimen (2D).

It can be seen from Figure 11 that there was a slight difference in the elastic section of each specimen, which maintained the same upward trend, and the yield point of the specimen showed little difference. In the strengthening stage, the ultimate load of the four specimens at failure was almost the same, with an average value of 188.1 kN. Compared with the type B-1 specimen in Figure 10, the bearing capacity was strengthened, but the failure mode was the same, and the steel bar of the specimen was broken. When the number of moving defects was 2, we can see from Figure 12 that the bearing capacity of four specimens of the two types was almost the same, and there was no significant difference in their ultimate displacement. The failure pattern was that the rebar was pulled off.

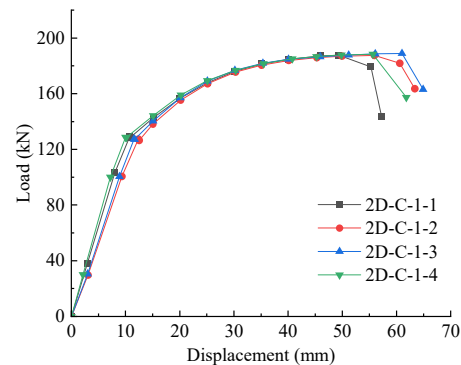


Figure 11. Load-displacement curve of type C-1 specimen (2D).

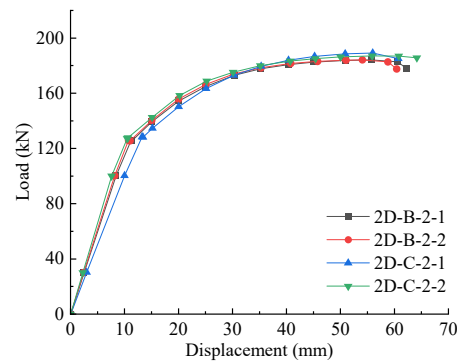


Figure 12. Load-displacement curves of type B-2 and type C-2 specimen (2D).

3.2.3. Specimen with Defect Length of 3D

Through the test of various specimens with a defect length of 3D, the test phenomenon was that the steel bar was pulled out. It can be seen from Figure 13 that in the elastic stage, there was little difference between the load values of four types of defects. In the yield stage, there was no significant difference in the load value, but the displacement of the 3D-A-1-1 specimen was large, indicating that it had a large slip. In the strengthening stage, the type A defects were concentrated on one side and the bond stress between the grouting material and the steel bar was unbalanced, which greatly reduced its ultimate bearing capacity. Although the bearing capacity of type B and C defects was higher than that of type A, there were many defects in the internal section of the grouting sleeve, which made the internal grouting material discontinuous. The stress of the grouting material at the defect was large, which reduced the ultimate bonding stress of the overall grouting material, and the steel bar was finally pulled out. The type H defect extended downward from the steel bar at the end of the sleeve, which ensured the continuity of the grouting material at the bottom and made its bearing capacity higher than that of other specimens. However, due to the reduction in the overall anchorage length, the contact between the grouting material and the sleeve interface was reduced, resulting in the reduction of the mechanical biting force, friction force and chemical cementation force. Therefore, the ultimate failure mode was that the steel bar was pulled out.

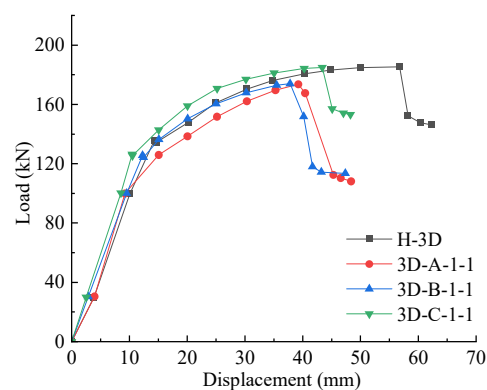


Figure 13. Comparison of load-displacement curves of various specimens (3D).

We can see from Figure 14 that the failure pattern of specimens was that the steel bar was pulled out, except for in the 3D-B-1-4 specimen. In the elastic stage, the load values of six curves had little difference. The average yield strength of the specimen was 127.9 kN. The curve slope changed slightly with the change in displacement value. The main reason was that there was a 1/4 overlap of type B defects in the vertical sleeve, and the movement of the single defect led to a different bond slip, which made the elastic section of specimens different. In the strengthening stage, there were great differences

among the specimens as follows: the early failure of the 3D-B-1-1 specimen and the 3D-B-1-6 specimen; the subsequent failure of the 3D-B-1-2 specimen, 3D-B-1-5 specimen and 3D-B-1-3 specimen; and the final failure of the 3D-B-1-4 specimen. To a certain extent, when moving a single defect, the vertical overlap of defects at both ends was reduced, which had little effect on the strengthening of the bearing capacity of the specimen, while the reduction in the vertical overlap of defects at the middle part greatly affected the bearing capacity of the specimen.

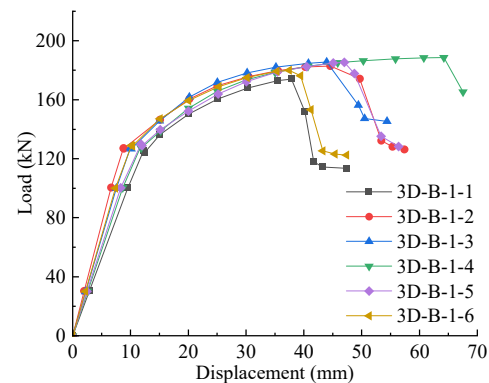


Figure 14. Load-displacement curve of type B-1 specimen (3D).

As shown in Figure 15, the failure pattern of the test sample was that the steel bar was pulled out, except for in specimens 3D-C-1-4 and 3D-C-1-5. Compared with the single moving defect specimen of 3D-B, the bond slip in the elastic stage was less, the load values of six curves had little difference and the curve slope had little difference. In the strengthening stage, the change of defects at the end and middle of the sleeve caused the early failure of the specimen. This was because under the uniaxial tension, the grouting materials at both ends were prone to stress concentration. If there were defects at this position, the bonding stress was further reduced. Therefore, the shear stress of the grouting material was greater than the bond strength, and the specimen was subject to sliding failure. The slight difference with the 3D-B single moving defect specimen was that the reduction in the vertical overlap of defects at both ends did not have a significant effect on improving the bearing capacity of the specimen, while the reduction in the vertical overlap of defects at the middle part improved the bearing capacity of the specimen.

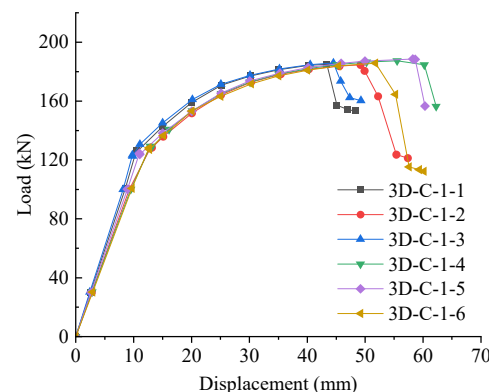


Figure 15. Load-displacement curve of type C-1 specimen (3D).

When multiple defects moved, except for the 3D-C-3-1 and 3D-C-4-1 specimens, which had steel bar fracture failure, the rest had steel bar pull-out failure. From Figure 16a,b, it can be concluded that in the elastic stage, except for 3-3 specimens with type B and type C defects, the difference between specimens was not large. The large slip of the 3-3 specimen in type B and type C led to the small slope of the linear segment. In the strengthening stage,

the pull-out failure of steel bars occurred in type B specimens, and the bearing capacity of 3D-B-3-1 and 3D-B-3-2 specimens was better, which showed that the failure force of defects near the end of the sleeve was small. Under the same defect size, the bearing capacity of type C defects was better than that of type B defects. This was because type C reduced the vertical overlap of defects to a greater extent and could better play the symmetry of defect-free parts to achieve stress balance and improve the bonding stress. The bearing capacity of 3-3 specimens with type B and type C defects was weak, and the ultimate bearing capacity was 173.65 kN and 184.85 kN, respectively, which once again confirms that the overlap of defects at the end and middle of the sleeve had a great effect on the quality of the specimen.

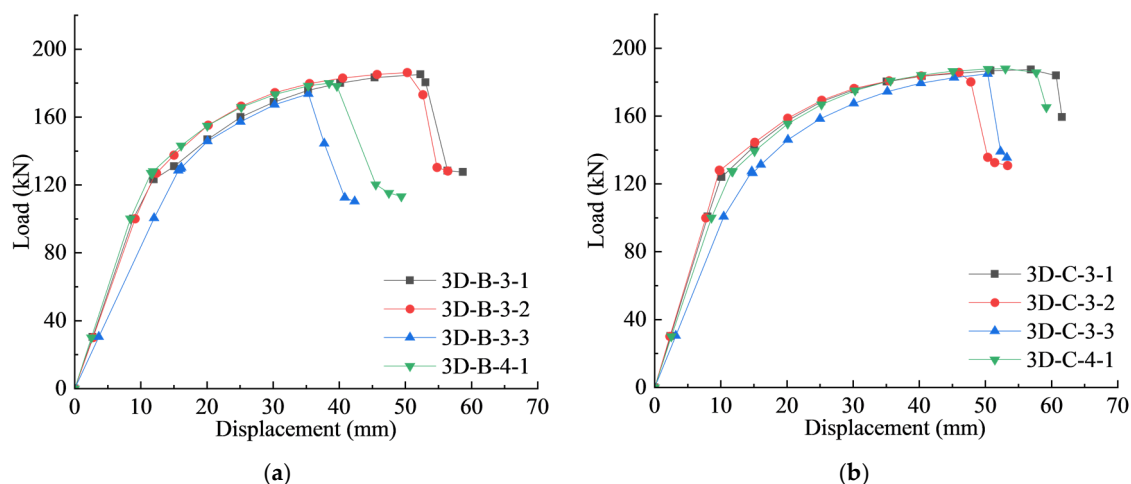


Figure 16. Load-displacement curves of multiple defects moving (3D): (a) type B; (b) type C.

3.3. Influence of Defects on Ultimate Bearing Capacity and Displacement

From Table 4, it can be seen that under the condition of the same defect length, the bearing capacity of the specimens with B and C defects was reduced to varying degrees compared with the full grouting, while the bearing capacity of the specimens with B defects was reduced by a large margin—3.64% on average. The main reason for this is that the vertical overlap of type B defects was large and concentrated defects appeared in the overlapping parts, which reduced the bond strength. From the perspective of displacement, the ultimate displacement of C-type defects was greater than that of B-type defects, and the ultimate displacement was positively correlated with the bearing capacity.

Table 4. Comparison of test data with defect length of 2D.

Test Specimen Number	Ultimate Bearing Capacity/kN	Reduce Amplitude	Displacement/mm	Increasing Extent	Failure Mode of Steel Bar
BM	189.83	0	54.7	0	Fracture
2D-B-1-1	185.12	2.48%	55.7	1.83%	Fracture
2D-B-1-2	183.10	3.64%	50.0	−8.44%	Fracture
2D-B-1-3	183.50	3.46%	50.1	−9.20%	Fracture
2D-B-1-4	185.25	2.50%	52.8	−3.79%	Fracture
2D-B-2-1	184.30	2.99%	55.7	1.89%	Fracture
2D-B-2-2	184.30	3.00%	54.1	−1.08%	Fracture
2D-C-1-1	187.65	1.18%	49.3	−9.98%	Fracture
2D-C-1-2	187.45	1.27%	55.9	2.43%	Fracture
2D-C-1-3	188.85	0.52%	61.0	11.27%	Fracture
2D-C-1-4	188.40	0.76%	55.6	1.48%	Fracture
2D-C-2-1	189.20	0.33%	55.9	2.16%	Fracture
2D-C-2-2	187.15	1.42%	55.9	2.15%	Fracture

Note: BM, the control group of the test, represents the specimen with full grouting.

It can be seen from Table 5 that when a single defect was moved along the circumferential direction, the specimens 3D-B-1-4, 3D-C-1-4 and 3D-C-1-4 underwent tensile failure of steel bars. This shows that under the same defect conditions, the grouting defect at the end of the sleeve had little effect on the bond strength of the specimen, while the grouting defect at the middle part had a great influence on the bond strength of the sleeve. When the two defects were moved along the circumferential direction, the specimens 3D-B-2-4 and 3D-C-2-4 also underwent tensile failure of the steel bar, and the above conclusions could again be drawn. From the perspective of displacement, when the defect length was 3D, the ultimate displacement of the specimen was greatly reduced, but compared with the C-type defect, the reduction in the B-type defect specimen was greater. With the increase in ultimate bearing capacity, the ultimate displacement of the specimen also increased.

Table 5. Comparison of test data with defect length of 3D.

Test Specimen Number	Ultimate Bearing Capacity/kN	Reduce Amplitude	Displacement/mm	Increasing Extent	Failure Mode of Steel Bar
BM	189.83	0	54.7	0	Fracture
3D-B-1-1	174.00	8.34%	37.8	−30.90%	Pull out
3D-B-1-2	182.95	3.95%	44.6	−26.72%	Pull out
3D-B-1-3	185.65	2.28%	43.9	−24.22%	Pull out
3D-B-1-4	188.65	0.64%	64.0	21.18%	Fracture
3D-B-1-5	185.40	2.35%	47.1	−11.88%	Pull out
3D-B-1-6	180.01	5.30%	37.4	−36.73%	Pull out
3D-C-1-1	185.02	2.67%	43.4	−30.21%	Pull out
3D-C-1-2	184.65	2.80%	49.2	−12.67%	Pull out
3D-C-1-3	185.90	2.13%	44.5	−20.73%	Pull out
3D-C-1-4	187.35	1.33%	55.5	1.80%	Fracture
3D-C-1-5	188.65	0.63%	58.2	6.31%	Fracture
3D-C-1-6	185.75	2.16%	51.8	−4.98%	Pull out
3D-B-2-1	182.35	4.03%	39.5	−29.34%	Pull out
3D-B-2-2	184.30	3.03%	46.0	−22.03%	Pull out
3D-B-2-3	185.91	2.13%	49.1	−12.17%	Pull out
3D-B-2-4	187.65	1.17%	57.9	6.52%	Fracture
3D-B-2-5	181.02	4.69%	39.1	−26.94%	Pull out
3D-C-2-1	185.10	2.61%	48.2	−16.62%	Pull out
3D-C-2-2	182.55	3.93%	41.3	−27.80%	Pull out
3D-C-2-3	186.35	1.91%	49.5	−12.59%	Pull out
3D-C-2-4	187.95	1.01%	53.3	−2.83%	Fracture
3D-C-2-5	181.03	4.68%	39.0	−29.46%	Pull out

Note: BM, the control group of the test, represents the specimen with full grouting.

4. Conclusions

Through uniaxial tensile tests on grouting sleeves, the following conclusions are drawn:

When the sleeve defect length is 1D and 2D, the steel bar of the specimen is broken. When the defect length is 3D, the test results show that with the different defect distribution types, a small part of the specimen is broken and the rest have steel bars pulled out.

In the specimen with a defect length of 2D, regarding the ultimate displacement of class B and class C specimens with the same defect type number, class B was less than class C. In the specimen with a defect length of 3D, the ultimate displacement increased with the increase in bearing capacity.

For the specimen with a defect length of 2D, the failure mode was steel bar fracture, and the bearing capacity of different defect distribution types was basically type $A < B < C \approx H$. There was little difference between the ultimate bearing capacity and displacement of specimens with one type of defect. For the specimen with a defect length of 3D, the bearing capacity of different defect distribution types was basically type

$A < B < C < H$. The bearing capacity of specimens with one type of defect was significantly different.

When moving defects, the vertical overlap of defects at both ends had little effect on the bearing capacity of the specimen, while the vertical overlap of defects at the middle part had a great influence on the bearing capacity of the specimen.

Author Contributions: Conceptualization, J.Z. and B.Y.; methodology, Y.Z. and Y.Y.; software, L.Y.; validation, J.C.; formal analysis, L.Y.; investigation, J.Z. and Y.Z.; resources, J.Z. and Y.Z.; data curation, B.Y.; writing—original draft preparation, L.Y. and J.C.; writing—review and editing, Y.Y. and B.Y.; visualization, L.Y. and J.C.; supervision, Y.Z. and Y.Y.; project administration, J.Z. and B.Y.; funding acquisition, J.Z. All authors have read and agreed to the published version of the manuscript.

Funding: This research was funded by the National Natural Science Foundation of China, grant number 12162010 and the Guangxi Science and Technology Plan Project, grant numbers Guike AD20159085 and Guike AA20302006.

Data Availability Statement: The data used to support the findings of this study are available from the corresponding authors upon request. The data are not publicly available due to privacy.

Conflicts of Interest: The authors declare no conflict of interest.

References

1. Ling, J.H.; Rahman, A.B.A.; Mirasa, A.K.; Hamid, Z.A. Performance of CS-sleeve under direct tensile load: Part 1: Failure modes. *Malays. J. Civ. Eng.* **2008**, *20*, 89–106.
2. Ling, J.H.; Rahman, A.B.A.; Ibrahim, I.S.; Hamid, Z.A. Behavior of grouted pipe splice under incremental tensile load. *Constr. Build. Mater.* **2012**, *33*, 90–98. [[CrossRef](#)]
3. Ling, J.H.; Rahman, A.B.A.; Ibrahim, I.S. Feasibility study of grouted splice connector under tensile load. *Constr. Build. Mater.* **2014**, *50*, 530–539. [[CrossRef](#)]
4. Wu, X.B.; Lin, F.; Wang, T. Experimental research on effects of grout age and types of steel bars on mechanical behavior of grout sleeve splicing for reinforcing bars. *Build. Struct.* **2013**, *43*, 77–82. (In Chinese)
5. Steuck, K.P.; Eberhard, M.O.; Stanton, J.F. Anchorage of large-diameter reinforcing bars in ducts. *ACI Struct. J.* **2009**, *106*, 506.
6. Sayadi, A.A.; Rahman, A.B.A.; Jumaat, M.Z.B.; Alengaram, U.J.; Ahmad, S. The relationship between interlocking mechanism and bond strength in elastic and inelastic segment of splice sleeve. *Constr. Build. Mater.* **2014**, *55*, 227–237. [[CrossRef](#)]
7. Chen, J.; Wang, Z.; Liu, Z.; Ju, S. Experimental investigation of mechanical behaviour of rebar in steel half-grouted sleeve connections with defects in water/binder ratio. *Structures* **2020**, *26*, 487–500. [[CrossRef](#)]
8. Liu, C.; Pan, L.; Liu, H.; Tong, H.; Yang, Y.; Chen, W. Experimental and numerical investigation on mechanical properties of grouted-sleeve splices. *Constr. Build. Mater.* **2020**, *260*, 120441. [[CrossRef](#)]
9. Xu, F.; Wang, K.; Wang, S.G.; Li, W.W.; Liu, W.Q.; Du, D.S. Experimental bond behavior of deformed rebars in half-grouted sleeve connections with insufficient grouting defect. *Constr. Build. Mater.* **2018**, *185*, 264–274. [[CrossRef](#)]
10. Zheng, G.Y.; Kuang, Z.P.; Xiao, J.Z.; Pan, Z.F. Mechanical performance for defective and repaired grouted sleeve connections under uniaxial and cyclic loadings. *Constr. Build. Mater.* **2020**, *233*, 112–233. [[CrossRef](#)]
11. Zhang, W.X.; Wang, J.; Zhang, J.Y.; Cao, Y.D.; Qin, P.; Yi, W.J. Experimental study on post-fire performance of half grouted sleeve connection with construction defect. *Constr. Build. Mater.* **2020**, *244*, 118–165. [[CrossRef](#)]
12. Wang, X. Influence of Grouting Material Content on Mechanical Properties of Grouting Connection of Steel Sleeve. Master's Thesis, Tongji University, Shanghai, China, 2016. (In Chinese).
13. Zhou, K.; Chen, Y.Q. Research on Construction Defects and Detection Methods of Steel Sleeve Grouting connection. *Constr. Technol.* **2020**, *6*, 69–72. (In Chinese)
14. Wang, T.J.; Zheng, G.Y. Computational Model Analysis on Mechanical Behavior of Grouted Sleeve Connector with Grouting Defect. *J. Jiamusi Univ. (Nat. Sci. Ed.)* **2018**, *36*, 196–200+205. (In Chinese)
15. Chen, X.N. Study on New-Type Grouted Deformed Pipe Splice. Master's Thesis, Southeast University, Shanghai, China, 2015. (In Chinese)
16. Zhao, J.; Du, Y.B.; Zhu, W.X. Finite element analysis of grouting coupler connection member. *Concrete* **2019**, *10*, 150–154. (In Chinese)
17. Li, X.M.; Gao, R.D.; Xu, Q.D.; Wang, Z.L.; Wang, M.Q.; Zhang, F.W. Experimental study on repairing grouting defects at different positions of sleeve of monolithic precast concrete structure. *Build. Struct.* **2019**, *49*, 93–97. (In Chinese)
18. Gao, R.D.; Li, X.M.; Zhang, F.W. Study on Influences of Grouting in Different Positions on Joint Strength of Steel Sleeve Grouting. *Constr. Technol.* **2019**, *48*, 116–119+124. (In Chinese)
19. Zheng, Q.L. *Experimental Study on Effects of Grouted Defects on Behaviors of Grout Sleeve Splicing and Specimens*; China Academy of Building Research: Beijing, China, 2017. (In Chinese)

20. Yu, Q.; Wang, Z.Q.; Bai, S.H.; Fan, B.X.; Zhang, Z.; Dong, J.M.; Chen, Z.H.; Gong, X. Tensile test and stress mechanism analysis of grouted sleeve lapping connectors for rebar. *J. Harbin Inst. Technol.* **2021**, *53*, 96–110. (In Chinese)
21. *JG/J 408-2013*; The Grouting Sleeve for Rebars Splicing. China Architecture & Building Press: Beijing, China, 2013.
22. *JG/J 398-2019*; The Grouting Sleeve for Steel Connection. China Architecture & Building Press: Beijing, China, 2019.
23. *JG/J 355-2015*; Technical Specification for Grout Sleeve Splicing of Rebars. China Architecture & Building Press: Beijing, China, 2015.

Disclaimer/Publisher's Note: The statements, opinions and data contained in all publications are solely those of the individual author(s) and contributor(s) and not of MDPI and/or the editor(s). MDPI and/or the editor(s) disclaim responsibility for any injury to people or property resulting from any ideas, methods, instructions or products referred to in the content.